Velocity Derivative Skewness in Isotropic Turbulence and its Measurement with Hot Wires

P. Burattini[1,3]**, P. Lavoie**[2]**, and R. A. Antonia**[3]

[1]Physique Statistique et des Plasmas
Université Libre de Bruxelles, B-1050 Brussels, BELGIUM

[2]Department of Aeronautics, Imperial College London, UK
[3]Discipline of Mechanical Engineering, University of Newcastle, NSW 2308, AUSTRALIA

Abstract

We investigate the effect of the hot wire resolution on measurements of the velocity derivative skewness in homogeneous isotropic turbulence. A single wire configuration (with different lengths and temporal sampling resolutions) is considered. Estimates of the attenuation, based on numerical data in box turbulence, are applied to experimental data taken in grid turbulence. It is found that the sampling resolution has a sizeable attenuation effect, while the length of the wire has a relatively minor impact. The corrected experimental values support the conclusion that the skewness is constant with the Reynolds number, in agreement with Kolmogorov's 41 theory.

Introduction

Homogeneous isotropic turbulence (HIT, hereafter) is characterized by a negative skewness of the velocity derivative $\partial u_i / \partial x_i$, where u_i is the velocity fluctuation component along x_i. As is customary, the skewness is defined by

$$S \equiv - \frac{\overline{\left(\frac{\partial u_i}{\partial x_i}\right)^3}}{\left[\overline{\left(\frac{\partial u_i}{\partial x_i}\right)^2}\right]^{3/2}} \qquad (1)$$

(note the negative sign). In HIT, the skewness represents the rate of production of vorticity through vortex stretching [12], and the non-zero value arises from the non-linearity of the Navier–Stokes equation. Given its significance, theoretical predictions of S and its dependence on the turbulence Reynolds number $R_\lambda (= \lambda u'/\nu$, where u' is the velocity fluctuation rms, λ is the Taylor microscale, and ν is the kinematic viscosity), have been extensively considered in the past. While Kolmogorov [8] (K41) argued that S should be constant, others predicted that it would either increase, based on intermittency arguments of Kolmogorov [9] (K62), or decrease [6], as R_λ increases. In particular, George [6] suggested that the product SR_λ should remain constant, as R_λ varies. The conflicting predictions arising from K41 and K62 generated a large amount of research work (see [18] for an account on different physical models relating skewness and intermittency). Nevertheless, Nelkin [14] noted that this issue remains unresolved. The behaviour of S has also been investigated experimentally [5, 17, 13] and numerically [11, 7, 1]; extensive collections of data for S in different flows are given in [17, 18]; see also the review [15]. Note that, to date, the values of S at the highest R_λ come from experiments.

Hot wires can provide accurate measurements of the skewness with a resolution that can not yet be matched by other experimental techniques. The spatial resolution of the probe might, nevertheless, affect negatively the estimate of S. In fact, the derivative of the velocity is dominated by the small scale motion (SSM), which is difficult to resolve accurately. Further, the time sampling resolution of the velocity signal has also an impact on the measurement of the SSM.

The loss of information due to averaging of the velocity fluctuations over the probe size and to finite time sampling can however be restored with analytical arguments. One needs to assume a functional form for the three-dimensional (3D) energy spectrum, E, and consider the actual geometrical size and wire arrangement of the probe. This approach, yielding corrections in terms of the velocity spectrum, was described by [19]. Although this method is probably the most common, there are also alternative procedures to compensate for the resolution loss. For example, Bremhorst [2] used the velocity correlation functions and relaxed the isotropy condition, while retaining homogeneity, see also [21].

Although corrections for the velocity fluctuation rms [19, 21], the mean energy dissipation rate [21], and the mean square vorticity or enstrophy [20, 22] have been reported and discussed in the literature (for a review see [22], mainly concerning the probe spatial resolution), the effect of the temporal and spatial resolutions of a probe for measuring S do not seem to have been discussed previously.

Using direct numerical simulations of turbulence, it is now possible to evaluate the effects due to finite spatial and temporal resolutions of a hot wire employed in the experiments. The probe is somewhat idealized in that its disturbance on the flow and the response to the parallel velocity component are neglected. Similar approaches were previously adopted in [16] and [21] for the channel flow, with particular attention to the variance of the velocity fluctuation and of its derivative (in a view to estimate the mean energy dissipation rate). To date, there is no parallel analysis for isotropic turbulence. And yet, for this flow the balance between kinetic energy decay and dissipation is exact, making it particularly suitable as a test case. It is also meaningful to assess the effect of resolution of hot wires for this fundamental flow, since a large amount of data has been collected in grid turbulence. In a recent paper [3], the effect of the sensor length of a cold wire probe for scalar measurements in isotropic turbulence was considered, by using direct numerical simulations (DNSs). Results showed that for lengths up to 15 times the Batchelor microscale, the mixed velocity-scalar derivative skewness was overestimated of up to 15%, while the scalar variance and mean dissipation rate were underestimated. Given the relevance of the velocity derivative skewness and the widespread use of hot wire anemometry for its measurement, in the present article we quantify the effect that the spatial and temporal resolutions of a single-wire (SW) have on the measurement of S.

Experimental and Numerical Details

Homogeneous isotropic turbulence is generated in a grid tunnel of open-circuit type. Five grids, differing in the geometry of the elements (including mesh size M, diameter of the elements d_e and solidity σ) and construction, are used; four of them have biplane elements, the fifth is a woven mesh (see table 1, for geometrical details). These grids produce different initial conditions and attain also different values of R_λ in the range 11,47.
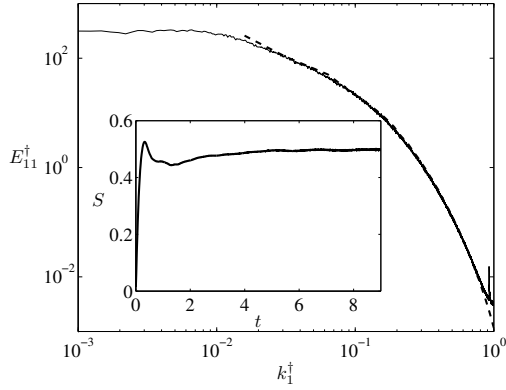
Figure 1: Comparison of 1D spectra measured by a single wire at $R_\lambda = 47$ with grid sq35 (—), and calculated from the simulation at $R_\lambda = 49$ ($--$). Inset: velocity derivative skewness during the temporal decay from simulations.

The grids are inserted immediately downstream of a contraction (area ratio of 9:1), and this is followed by the working section, 2.4 m long and of square cross-section (width 350 mm). Zero pressure gradient in the test section is ensured by adjusting the floor of the tunnel, and measurements are made along the tunnel centreline — more details can be found in [10].

Symbol	Name	Grid type (elem., constr.)	M (mm)	d_e (mm)	σ –
$\triangledown$ — $\cdot$	sq35	square, biplane	24.76	4.76	0.35
$\square$—	rd35	round, biplane	24.76	4.76	0.35
$\diamondsuit\cdots$	rd35b	round, biplane	24.76	4.76	0.35
$\bigcirc$ – –	rd44	round, biplane	24.76	6.35	0.44
$\triangleleft$ – –	rw35	round, woven	4.25	0.825	0.35

Table 1: Main parameters for the grids.

The wires are operated by in-house constant temperature circuits at an overheat ratio of 1.5. Buck-and-gain conditioning is applied to the velocity signals, before they are low-pass filtered at a cut-off frequency f_c; this varies depending on the grid and measurement location. The cut-off frequency corresponds to the onset of electronic noise and is roughly equal to $f_k \equiv U_1/\eta$, the Kolmogorov frequency. Sampling is implemented at a frequency $f_s \geq 2f_c$, and a 16 bit A/D converter is used to digitize the data. The single wire response is fitted to a third-order polynomial. The mean dissipation rate ε is estimated from the decay rate of the kinetic energy; the rms velocity is corrected for spatial resolution, using the spectral correction method of [21]. The value of ε is then used to obtain η, employed in the normalisation of the probe size. Taylor's hypothesis, i.e. $x_1 = -U_1 t$, is used for the time-space conversion, assuming that the flow is locally homogeneous. In the experiment, the streamwise location is denoted by x_M, the distance from the grid location normalised by the grid mesh size. In the following, a dagger denotes normalisation by Kolmogorov scales.

For the experiment with the grid rw35 — where η is the smallest — a single wire with $d_w = 1.26\ \mu$m and $l \simeq 0.25$ mm is used. For all the other grids, the single wire has $d_w = 2.54\ \mu$m and $l \simeq 0.5$ mm, see table 1. All wires are etched from Wollaston (Pt-10% Rh).

Temporally-decaying isotropic turbulence is simulated in a periodic box of 256^3 nodes, by solving the Boltzmann equation on a lattice, see [4]. Computations are performed in double precision on a cluster of PCs located at the University of Newcastle,
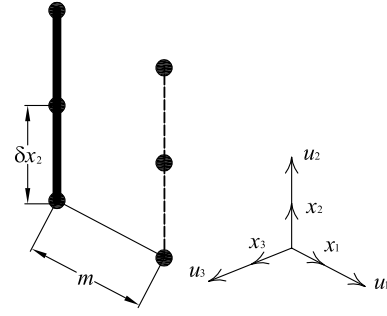
Figure 2: Schematic of the velocity averaging using three nodes of the computed field, to represent one wire.

where the wind tunnel is also situated.

Experimental and numerical spectra, compared in figure 1, are nearly identical. The temporal profile of S, inset of figure 1, starts from zero at the beginning of the simulations, reflecting the provisional and unphysical velocity field, but quickly settles around 0.5. It was verified that the estimates of the skewness from the three velocity components are identical, within statistical fluctuations. The velocity field used in the following corresponds to $t = 8.5$, when the turbulence is fully developed, and the maximum resolved wavenumber (normalised by η) is 3.28, at $R_\lambda = 21$.

Results

The resolution effects of the SW are estimated from the numerical data by considering the virtual probe oriented like in figure 2. Values of the velocity, taken at a set of nodes which correspond to the shape of the SW are combined in physical space to provide a filtered velocity field. The effect of line averaging on u_1 is given by

$$u'_1(x_1,x_2,x_3) = \frac{1}{n+1} \sum_{i=0,n} u_1(x_1, x_2 + i\delta x_2, x_3), \qquad (2)$$

where $n\delta x_2$ represents the length of the wire l, δx_2 being the numerical mesh increment (equal in the three directions). The effect of reduced spatial sampling on the spatial derivative $\partial u'_1/\partial x_1$ is given by the finite difference (equivalent to a zero-order hold sampling)

$$\frac{u'_1(x_1 + j\delta x_1, x_2, x_3) - u'_1(x_1, x_2, x_3)}{j\delta x_1}, \qquad (3)$$

where $j\delta x_1$ (j positive integer) represents the spatial increment m.

The attenuation effect on S of the virtual SW, estimated from the numerical data via (2) and (3), is given in figure 3. The curves are normalised by the skewness calculated using the fully resolved field. The effect of the undersampling in the x_1-direction is dominant over the effect of line averaging. Note that this latter leads, for very small values of $m^\dagger$, to a tiny overestimation of the skewness. This effect is displayed also by the mixed velocity-scalar derivative skewness [3].

Figure 4 shows the distributions of $l^\dagger$ and $m^\dagger$ during the grid turbulence decay, for all the measurements performed. Although the size of the probes is fixed, η increases in the streamwise direction, hence the decreasing trends. Also, in the experiment the sampling frequency is reduced in a stepwise manner, while the probe is traversed in the streamwise direction. This explains the saw-tooth profile of $m^\dagger$. With the present values of $l^\dagger$ and
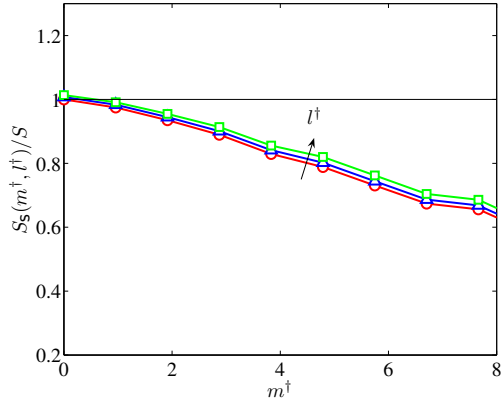
Figure 3: Effect of undersampling and wire length on S_s from simulations: —○, $l^\dagger = 0$; —△, $l^\dagger = 1.92$; —□, $l^\dagger = 3.83$.
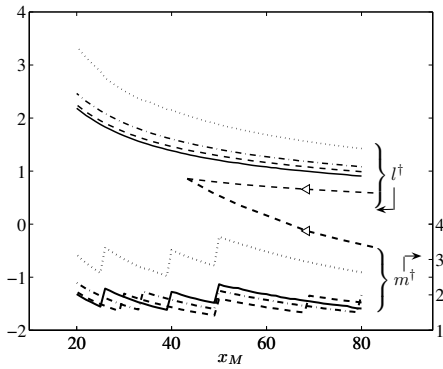
Figure 4: Profiles of the normalised size ($l^\dagger$) and sampling rate ($m^\dagger$) for the SW, during the grid turbulence decay. —, rd35; −−, rd44; −·, sq35; ···, rd35b; ◁ −−, rw35.
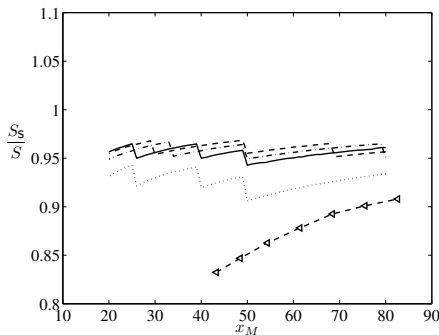
Figure 5: Correction factors for the SW probe used in the experiment, as estimated from simulations. —, rd35; −−, rd44; −·, sq35; ···, rd35b; ◁ −−, rw35.
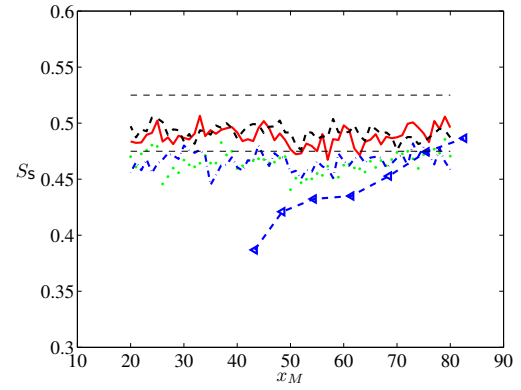
Figure 6: Uncorrected values of the skewness measured with the SW. —, rd35; −−, rd44; −·, sq35; ···, rd35b; ◁ −−, rw35. The horizontal dashed lines are at ±5% of the ensemble average ($\simeq 0.5$) of the corrected values, see figure 7.
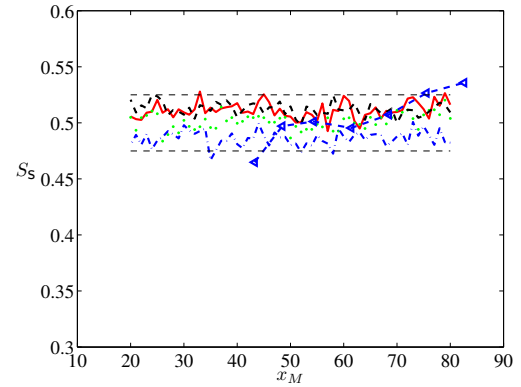
Figure 7: Corrected values of the skewness measured with the SW. —, rd35; −−, rd44; −·, sq35; ···, rd35b; ◁ −−, rw35. The horizontal dashed lines are at ±5% of the ensemble average ($\simeq 0.5$).

$m^\dagger$, and using the numerical results of figure 3, the attenuation of S caused by the resolution of the real SW can be estimated. Figure 5 shows that the attenuation amounts to around 5% for all cases except rw35, for which it lies between 10% and 15%.

The measured values of S during the decay are given in figure 6. Note the relatively large scatter between the data obtained from different grids. By applying the correction factors of figure 5 to the measured values of S_s in figure 6, the skewness values are corrected for the attenuation of the probe. The new values, figure 7, are around 0.5 (±5%) for nearly all points and all cases.

Figure 8 shows the product of the skewness measured by the SW (and corrected for the resolution) and the Taylor microscale Reynolds number. The product $S_s R_\lambda$ decreases slightly in the streamwise direction. This reduction is clearly an effect of the decay of R_λ, since S_s is nearly constant within this interval, as seen in figure 7.

Conclusions

We estimated the effect of resolution for a single wire on the measurement of the velocity derivative skewness. The turbulent flow considered is homogeneous and isotropic. The present conclusions are based on data from numerical simulations in box turbulence and experiments in grid turbulence (both at low R_λ). Results show that for this probe, the effect of the spatial
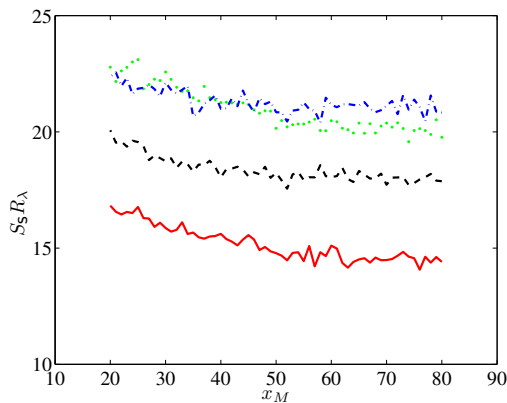
Figure 8: Profile of the product S_sR_λ during the grid turbulence decay, using the SW data corrected for resolution. —, rd35; −−, rd44; −·, sq35; ···, rd35b.

undersampling is more important than line averaging. Further, while increasing m attenuates S, for small values of m, the effect of l yields an overestimation of S.

Since the corrected experimental values of the skewness from the single hot wire are constant with respect to x_M, the product SR_λ decreases slightly with x_M, reflecting the slight decrease in R_λ. This is at variance with a recent similarity proposal [6] implying that SR_λ should remain constant during the decay.

References

[1] Antonia, R. A. and Orlandi, P., Similarity of decaying isotropic turbulence with a passive scalar, *J. Fluid Mech.*, **505**, 2004, 123–151.

[2] Bremhorst, K., The effect of wire length and separation on X-array hot-wire anemometer measurements, *IEEE Trans. Instrum. Meas.*, **IM-21**, 1972, 244–248.

[3] Burattini, P., Kinet, M., Carati, D. and Knaepen, B., Corrections for underresolved scalar measurements in turbulent flows using a DNS database, *Exp. Fluids*, **43**, 2007, 31–37.

[4] Burattini, P., Lavoie, P., Agrawal, A., Djenidi, L. and Antonia, R. A., Power law of decaying homogeneous isotropic turbulence at low Reynolds number, *Phys. Rev. E*, **73**.

[5] Champagne, F. H., The fine-scale structure of the turbulent velocity field, *J. Fluid Mech.*, **86**, 1978, 67–108.

[6] George, W. K., The decay of homogeneous isotropic turbulence, *Phys. Fluids A*, **4**, 1992, 1492–1509.

[7] Gotoh, T., Fukayama, D. and Nakano, T., Velocity field statistics in homogeneous steady turbulence obtained using a high-resolution direct numerical simulation, *Phys. Fluids*, **14**, 2002, 1065–1081.

[8] Kolmogorov, A. N., Dissipation of energy in the locally isotropic turbulence, *Dokl. Akad. Nauk SSSR*, **32**, 1941, English translation in *Proc. R. Soc. Lond.* A 434 (1991) 15–17.

[9] Kolmogorov, A. N., A refinement of previous hypotheses concerning the local structure of turbulence in a viscous incompressible fluid at high Reynolds number, *J. Fluid Mech.*, **13**, 1962, 82–85.

[10] Lavoie, P., Djenidi, L. and Antonia, R., Effects of initial conditions in decaying turbulence generated by passive grids, *J. Fluid Mech.*, **585**, 2007, 395–420.

[11] Mansour, N. N. and Wray, A. A., Decay of isotropic turbulence at low Reynolds number, *Phys. Fluids*, **6**, 1994, 808–814.

[12] Monin, A. S. and Yaglom, A. M., *Statistical Fluid Mechanics: Mechanics of Turbulence*, volume 2, MIT Press, 1975.

[13] Mydlarski, L. and Warhaft, Z., On the onset of high-Reynolds-number grid-generated wind tunnel turbulence, *J. Fluid Mech.*, **320**, 1996, 331–368.

[14] Nelkin, M., Universality and scaling in fully developed turbulence, *Advances in Physics*, **43**, 1994, 143–181.

[15] Sreenivasan, K. R. and Antonia, R. A., The phenomenology of small-scale turbulence, *Ann. Rev. Fluid Mech.*, **29**, 1997, 435–472.

[16] Suzuki, Y. and Kasagi, N., Evaluation of hot-wire measurements in wall shear turbulence using a direct numerical simulation database, *Exp. Therm. Fluid Sci.*, **5**, 1992, 69–77.

[17] Tavoularis, S., Bennett, J. C. and Corrsin, S., Velocity-derivative skewness in small Reynolds number, nearly isotropic turbulence, *J. Fluid Mech.*, **88**, 1978, 63–69.

[18] Van Atta, C. W. and Antonia, R. A., Reynolds number dependence of skewness and flatness factors of turbulent velocity derivatives, *Phys. Fluids*, **23**, 1980, 252–257.

[19] Wyngaard, J. C., Measurement of small-scale turbulence structure with hot wires, *J. Phys. E: Sci. Instrum.*, **1**, 1968, 1105–1108.

[20] Wyngaard, J. C., Spatial resolution of the vorticity meter and other hot-wire arrays, *J. Phys. E: Sci. Instrum.*, **2**, 1969, 983–987.

[21] Zhu, Y. and Antonia, R. A., Effect of wire separation on X-probe measurements in a turbulent flow, *J. Fluid Mech.*, **287**, 1995, 199–223.

[22] Zhu, Y. and Antonia, R. A., The spatial resolution of hot-wire arrays for the measurement of small-scale turbulence, *Meas. Sci. Technol.*, **7**, 1996, 1349–1359.